PHYSICAL REVIEW B **81**, 064506 (2010)

Microwave surface impedance measurements of $Tl_xPb_{1-x}Te$: A proposed negative-U induced superconductor

P. J. Baker, R. J. Ormeno, and C. E. Gough
School of Physics and Astronomy, University of Birmingham, Edgbaston, Birmingham B15 2TT, United Kingdom

Y. Matsushita
Geballe Laboratory for Advanced Materials and Department of Materials Science and Engineering, Stanford University, Stanford, California 94305, USA

I. R. Fisher
Geballe Laboratory for Advanced Materials and Department of Applied Physics, Stanford University, Stanford, California 94305, USA

(Received 6 November 2009; revised manuscript received 20 January 2010; published 16 February 2010)

The microwave surface impedance of the proposed negative-U induced superconductor Tl(1.4%)PbTe has been measured for a number of single crystals at several frequencies from 4.5 to 15.2 GHz in both the zero-field and mixed superconducting states. For crystals with the best-quality surfaces, R_s and X_s at low temperatures showed no significant power-law T dependence. From the low-temperature values of X_s, we extracted $\lambda(0)=1.9\pm0.2$ μm, in good agreement with rigid-band model predictions. A coherence peak was observed in σ_1 below T_c consistent with BCS predictions. However, the observed temperature dependence of the superfluid fraction $[\lambda(0)/\lambda(T)]^2$ fitted BCS predictions best if a somewhat larger value of $\lambda(0)=2.7$ μm was assumed, which may be associated with remanent surface defects in even our best sample. In addition to investigating the field dependence of the microwave properties in the mixed state, a B_{c3} transition region was observed. The absence of a significant power-law temperature dependence at low temperatures in our best sample and the observation of a B_{c3} transition are strongly suggestive of conventional s-wave superconductivity.

DOI: 10.1103/PhysRevB.81.064506 PACS number(s): 74.25.F−, 78.70.Gq, 74.70.Dd

I. INTRODUCTION

The T_c (1.4 K) of the superconducting semiconductor Tl-doped PbTe ($Tl_xPb_{1-x}Te$) for $x=1.4\%$ is remarkably high for such a low carrier density[1] $\sim10^{20}$ cm^{-3}. It has recently been suggested that electron pairing is induced by quantum fluctuations between degenerate Tl charge states of Tl^{1+} and Tl^{3+}, which corresponds to pairs of holes hopping on and off the Tl sites.[2,3] The degenerate states are a product of the large negative-U associated with the Tl impurity.[4] An upturn in the dc resistivity (ρ_{dc}) above T_c appears to support such a model, as the degenerate states are analogous to the degenerate spin states of a Kondo metal. Calculations by Dzero *et al.*[5] have shown that BCS-type superconductivity is indeed possible in this "charge Kondo" regime.

Here we present microwave measurements of the complex surface impedance, $Z_s=R_s+iX_s$, of single-crystal samples of Tl(1.4%)PbTe at 4.5, 8.5, 10.7, and 15.2 GHz. Microwave measurements have proved to be a useful probe of superconducting mechanisms in novel materials. The surface resistance $R_s(T)$ reflects the losses from any unpaired electrons while the surface reactance $X_s(T)$ is directly proportional to the effective penetration depth $\lambda(T)$ determined by the number of superconducting electrons. In principle, the temperature dependence of these parameters can provide evidence for unconventional behavior[6] such as nodes,[7] strong anisotropy,[8] or multiband-energy gaps.[9] Furthermore, by measuring the absolute values of R_s and X_s, an accurate estimate of $\lambda(0)$ can be made. For Tl-doped PbTe, such a measurement allows a direct comparison with the theoretical predictions of a rigid band model.[3] Our measurements provide strong evidence for conventional s-wave BCS pairing.

II. MEASUREMENTS

Single crystals, up to a few millimeters in size, were grown using the unseeded vapor transport method.[3] Electron microprobe analysis using PbTe, Te, and Tl_2Te standards, on similar crystals to those used in this investigation, revealed a homogeneous Tl content of $x=1.4\pm0.1\%$ consistent with the chemical composition.

A cavity perturbation method[10] was used to measure the temperature dependence of the microwave surface impedance $Z_s(T)$. Small single crystals (≈0.5 mm^3) were glued to the end of a sapphire rod and positioned at the center of a high-Q ($\approx10^5$) dielectric resonator operating in a TE_{01n} mode with the sample in a uniform microwave field. The measured microwave properties were reproducible from run to run on cycling between room and low temperatures, confirming the mechanical and thermal stability of the sample support system.

An adiabatic demagnetization refrigerator or a pumped ^{3}He bath were used to cool the sample to ~100 mK and ~300 mK, respectively. A hot-finger technique[11] was used to control the sample temperature independently from that of the cavity, which was held constant at ~1.5 K. Small changes in the resonant frequency $\Delta f_0(T)$ and bandwidth $\Delta f_B(T)$ were then measured. $R_s(T)$ and $\Delta X_s(T)$ were derived using the perturbation formulas, $R_s(T)+i\Delta X_s(T)=\Gamma[\Delta f_B(T)$

$-2i\Delta f_0(T)]$, where Γ is a geometrical factor dependent on the microwave field at the sample location. To avoid inherent problems of drifts in the cavity frequency over long periods of time, all measurements were repeatedly made relative to a standard sample temperature (typically 1.0 K). Cavity background bandwidths were measured separately in the absence of a sample and were subtracted from measurements with the sample present.

In principle, the local equation

$$R_s = X_s = \sqrt{1/(2\omega\mu_0\rho_{\rm dc})} \tag{1}$$

in the normal state can be used in conjunction with measurements of $\rho_{\rm dc}$ to determine Γ indirectly and hence obtain absolute values of R_s and X_s. In our analysis we used $\rho_{\rm dc}$ measurements taken by Matsushita *et al.*[2] These were taken on a number of crystals, including the ones given here. We used a nominal value for $\rho_0 = 0.9 \pm 0.1$ mΩ cm and carried the statistical error though in our derivation of R_s and X_s. The resolution of our measurements enabled us to confirm the small upturn in normal-state resistance at low temperatures observed by Matsushita *et al.*,[2] which suggested the possibility of charge Kondo pairing. However the analysis of our measurements was complicated because of problems from finite-size effects, as the smallest crystals used were not much larger than the normal-state skin depth.

The accuracy, reproducibility, and analysis of our technique were tested by measurements on a Nb sample of known resistivity and similar dimensions to the measured samples. Such measurements were consistent with BCS predictions, with an exponential temperature dependence of both R_s and X_s at low temperature, with $f_b(T \to 0)$ falling to the measured cavity background value.

III. RESULTS

A. Surface impedance

Preliminary measurements in the superconducting state gave a power-law T dependence of $R_s(T)$ and $X_s(T)$ at low temperature, suggesting an order parameter with nodes. However, it became apparent that this was due to surface defects, possibly associated with the tendency of PbTe to flake along {100} planes. This led to strongly power-dependent measurements, typical of weak-link behavior. To confirm this, we purposely roughened the surface of a sample. This resulted in a dramatically increased quasilinear T dependence of R_s and X_s below ~ 0.7 K. No way could be found to improve sample surface quality by chemical polishing. We therefore selected samples for detailed analysis having the smoothest surfaces on optical inspection. The crystal C5 (the fifth crystal extracted from the C-growth batch) with the smoothest optical surfaces also had the lowest quasiexponential losses at low temperatures.

The temperature dependence of R_s and X_s for this sample, normalized to their values at T_c, are shown in Fig. 1. For comparison, we also show measurements for B1 (a crystal with less high-quality surfaces) and C2 (a crystals with purposely abraded surfaces). The solid line represents the ideal BCS predictions.

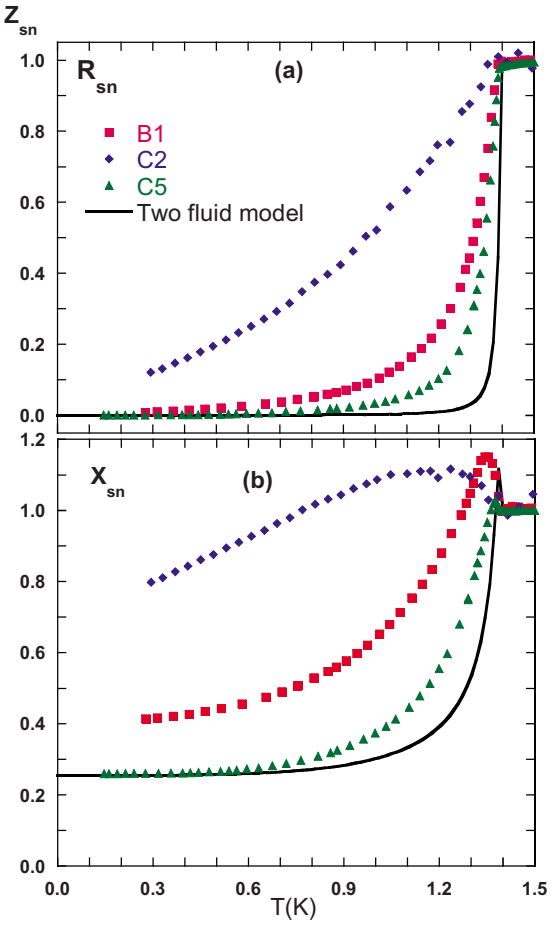

FIG. 1. (Color online) Plots of (a) R_{sn} and (b) X_{sn} normalized at T_c for Tl(1.4%)PbTe, taken at 10.7 GHz. The solid line represents the ideal BCS predictions.

The measurements shown Fig. 1 illustrate a very strong dependence on surface quality, approaching ideal s-wave BCS behavior for the sample with the smoothest surface (C5). In particular, there is no significant power-law T dependence at low temperatures, which might otherwise have suggested nonconventional pairing with nodes in the order parameter.

At higher temperatures, the agreement with the BCS predictions is less good. One particularly interesting feature is the peak in X_{sn} just below T_c. A similar peak was observed previously in superconducting Sr_2RuO_4 and was attributed to an initial decrease in screening from charge carriers as they condense into the superfluid state.[12] Such peaks are only predicted for highly conducting metals with a very short normal-state skin depth. For a poorly conducting metal such as Tl-doped PbTe, any such peak would be very narrow, as shown in Fig. 1(b). The very much broader observed peaks seems likely to be associated with weak-link behavior. Evidence for this is supported be the increasing microwave power dependence of measurements near T_c with surface roughness and the rapid suppression of the peak on the application of relatively small magnetic fields. In all the measurements reported here, the microwave power levels were well below the level at which nonlinear behavior was first observed.

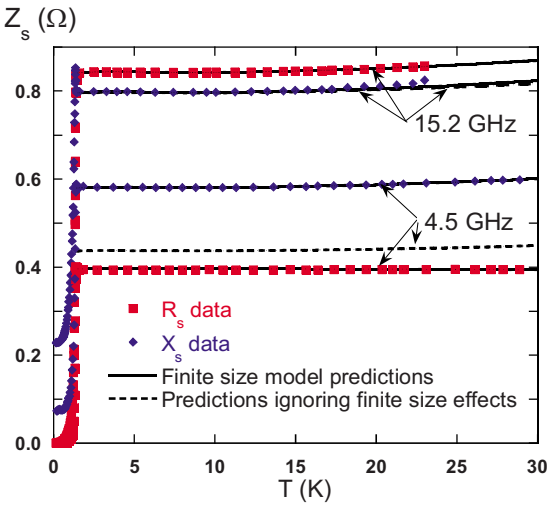

FIG. 2. (Color online) Plots of R_s and X_s in the normal state at 4.5 and 15.2 GHz for C5, where solid line fits have been made using the finite-size model (Ref. 13), with sample thickness of $c \sim 50$ μm. Dashed lines give the predictions ignoring finite-size effects, where $R_s = X_s$, see Eq. (1).

B. Low-temperature penetration depth

The temperature dependence of the microwave properties in the superconducting state involve the real and imaginary parts of the conductivity σ_1 and σ_2. These can be determined from measurements of R_s and X_s using the following relationships:

$$\sigma_1(T) = \omega\mu_0 \frac{2R_s(T)X_s(T)}{[R_s(T)^2 + X_s(T)^2]^2} \tag{2}$$

and

$$\sigma_2(T) = \omega\mu_0 \frac{X_s(T)^2 - R_s(T)^2}{[R_s(T)^2 + X_s(T)^2]^2}. \tag{3}$$

$\lambda(T)$ can then be derived using

$$\lambda(T) = [\omega\mu_0\sigma_2(T)]^{-1/2}. \tag{4}$$

Obtaining data for σ_1, σ_2, and $\lambda(0)$ relies on accurate absolute measurements of R_s and X_s. The usual method for obtaining absolute R_s and X_s values is to fit the data above T_c to the normal-state values determined by the dc conductivity [Eq. (1)]. However, our best crystal was very small, with a thickness of only ~ 50 μm—comparable to the normal-state skin depth, requiring corrections for the finite size. This leads to strongly frequency-dependent values of R_s and X_s in the normal state, as illustrated in Fig. 2. The absolute values of the plotted data have been calculated assuming a thin rectangular slab model[13] of thickness ~ 50 μm, in qualitative agreement with the measured thickness of the rather irregularly shaped crystal under an optical microscope. The curves in Fig. 2 show how finite-size effects can alter the temperature dependence and absolute values of R_s and X_s from their thick slab values, where $R_s = X_s$. In particular, finite-size effects alter the derived value of X_s used to estimate $\lambda(0)$. Corrections for such effects have therefore been made, as illustrated in Fig. 2.

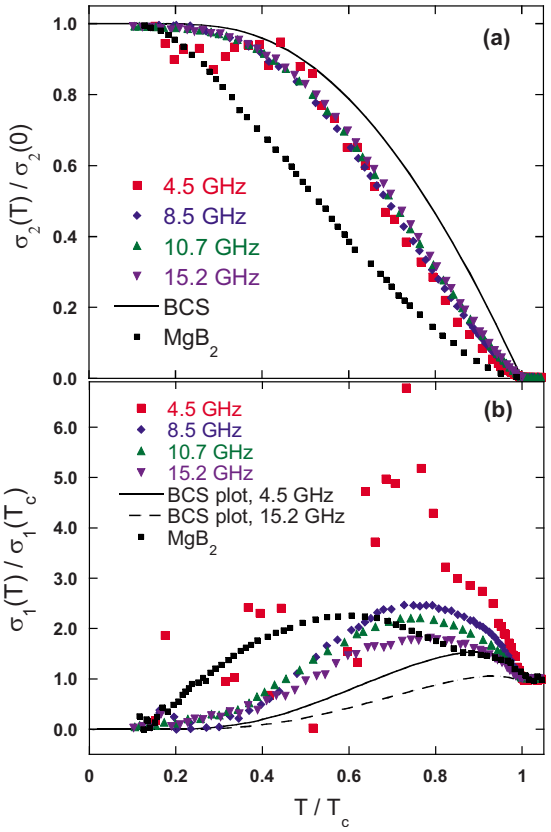

FIG. 3. (Color online) Plots of (a) $\sigma_2(T)/\sigma_2(0) = [\lambda(0)/\lambda(T)]^2$ and (b) $\sigma_1(T)/\sigma_1(T_c)$ for $\lambda(0) = 1.9$ μm. Also shown are the predictions from BCS theory and MgB_2 data from Jing *et al.* (Refs. 9 and 17).

The low-temperature penetration depth $\lambda(0)$ was calculated from the finite-size corrected X_s data using $X_s(0) = \omega\mu_0\lambda(0)$ and extrapolated values of $X_s(0)$. Using the highest-frequency measurements, where corrections for finite-size effects are smallest, and assuming an effective sample thickness of 50 μm, we obtained a value for $\lambda(0) = 1.9 \pm 0.2$ μm in excellent agreement with estimates based on the Hall effect data assuming a rigid band model,[3] giving $\lambda(0) = 1.9 \pm 0.5$ μm. At lower frequencies we assumed the same value for $\lambda(0)$, which served to define X_s on an absolute scale. This enabled us to make a more accurate estimate for the effective thickness. The resulting measurements shown in Fig. 2 have been plotted using a refined value for the effective thickness of 53 μm.

C. Temperature dependence of superconducting parameters

To obtain accurate values of σ_1 and σ_2 we have assumed the average value for $\lambda(0)$ of 1.9 μm at all frequencies. This then fixes the absolute values of R_s and X_s at low temperatures. The resulting values for $\sigma_2(T)/\sigma_2(0) = [\lambda(0)/\lambda(T)]^2$ (the superfluid fraction) and $\sigma_1(T)/\sigma_1(T_c)$ are plotted in Fig. 3. Also shown are the predictions for a weakly coupled BCS superconductor in the dirty limit (for example, Tinkham[14]). The $\sigma_1(T)/\sigma_1(T_c)$ plots were calculated using code given in Zimmerman *et al.*[15] and Marsiglio,[16] using a value of $\Delta(0) = 1.76k_BT_c$.

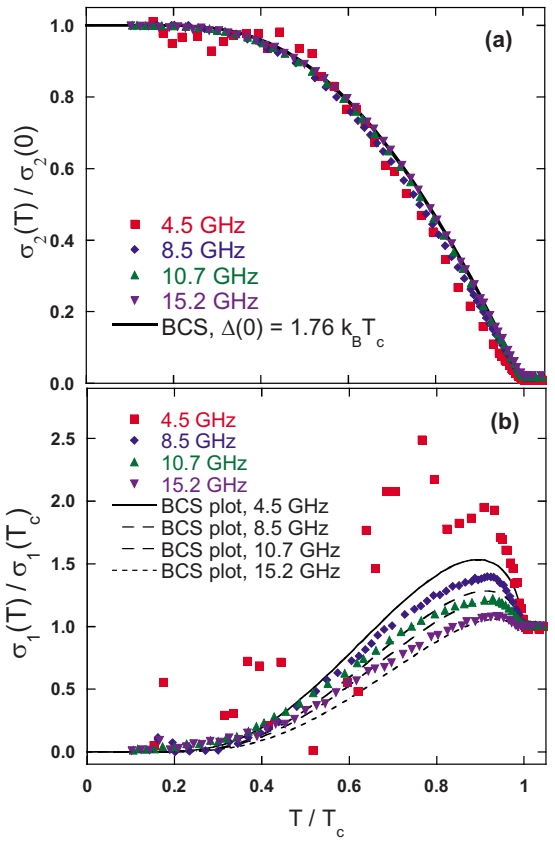

FIG. 4. (Color online) Plots of (a) $\sigma_2(T)/\sigma_2(0)=[\lambda(0)/\lambda(T)]^2$ and (b) $\sigma_1(T)/\sigma_1(T_c)$ for $\lambda(0)=2.7$ μm. Also shown are the predictions from BCS theory.

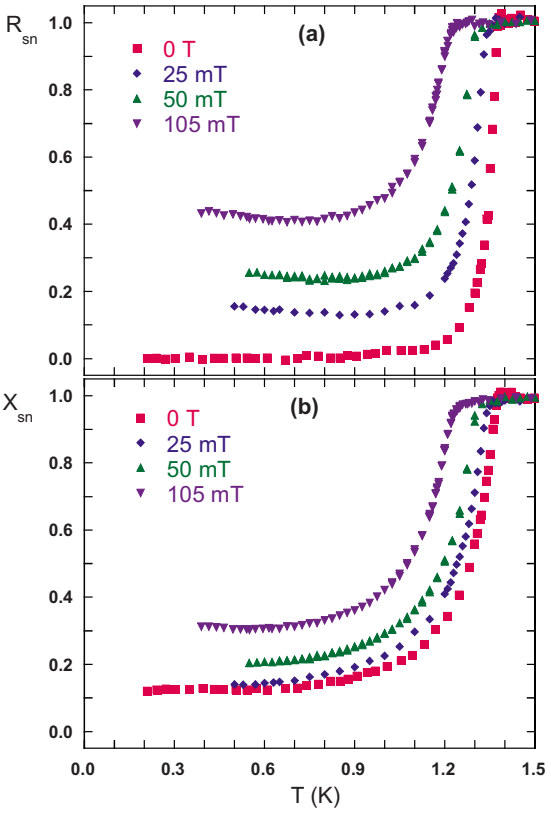

FIG. 5. (Color online) R_{sn} and X_{sn} verses T, for sample C5, in applied magnetic field B, at 4.5 GHz.

Importantly, the deduced values for the superfluid fraction $[\lambda(0)/\lambda(T)]^2$ at all frequencies lie on top of one another. However, the data fall somewhat below the BCS predictions in the dirty limit, assuming $\Delta(0)=1.76k_BT_c$. The experimental data for $\sigma_1(T)/\sigma_1(T_c)$ exhibit somewhat larger peaks below T_c than the frequency-dependent coherence peaks predicted by BCS theory in the dirty limit, possibly due to residual surface imperfections. We note that similar, but even larger departures from BCS predictions have been observed[9,17,18] for the two-band superconductor MgB_2, which might suggest multiband superconductivity in this compound also.

It should be noted that, had we assumed a value for $\lambda(0)$ of 2.7 μm, we would have obtained almost perfect agreement with BCS predictions for $\sigma_2(T)/\sigma_2(0)=[\lambda(0)/\lambda(T)]^2$ and an improved agreement for $\sigma_1(T)/\sigma_1(T_c)$, particular for the more accurate higher-frequency measurements, as shown in Fig. 4. However, such a value for $\lambda(0)$ is considerably larger than the value $(1.9\pm0.2$ μm) obtained from our microwave measurements and estimated from Hall measurements.[3]

IV. MEASUREMENTS IN APPLIED FIELDS

Several measurements were made on sample C5 at 4.5 and 15.2 GHz, in an applied magnetic field parallel to the microwave magnetic field. The data showed no observable differences between zero-field-cooled (FC) and FC measurements, implying the magnetic-flux lines move relatively freely into and out of the material. Furthermore, reverse field measurements gave identical results, showing no signs of ambient or trapped fields which might affect the field dependence at low fields.

Normalized R_s and X_s measurements at 4.5 GHz for relatively modest fields are shown in Fig. 5. The decrease in T_c with increasing magnetic field is consistent with previous measurements by Matsushita *et al.*[3] giving extrapolated values of $B_{c2}(0)\approx600$ mT.

At the transition to the mixed state in an applied field, both R_s and X_s decrease from their normal-state values. At low temperatures, the presence of flux lines results in a field dependent increase in both R_s and X_s. On increasing temperature, the additional contributions decrease, particularly for R_s, before increasing toward their normal-state values. A similar field dependence was observed at 15.2 GHz.

More extensive mixed-state measurements were also performed at 10.7 GHz on a slightly larger sample A3 with a somewhat lower-quality surface. The normalized R_s and X_s data for this sample are shown in Fig. 6. Finite-size corrections in this case were unnecessary due to the larger size of sample A3.

In both samples the zero-field peak in X_s at T_c, which we have associated with weak-link behavior, was rapidly suppressed by the application of quite modest fields ($\sim$50 mT). Over the rest of the temperature range, the temperature and field dependence is consistent with microwave

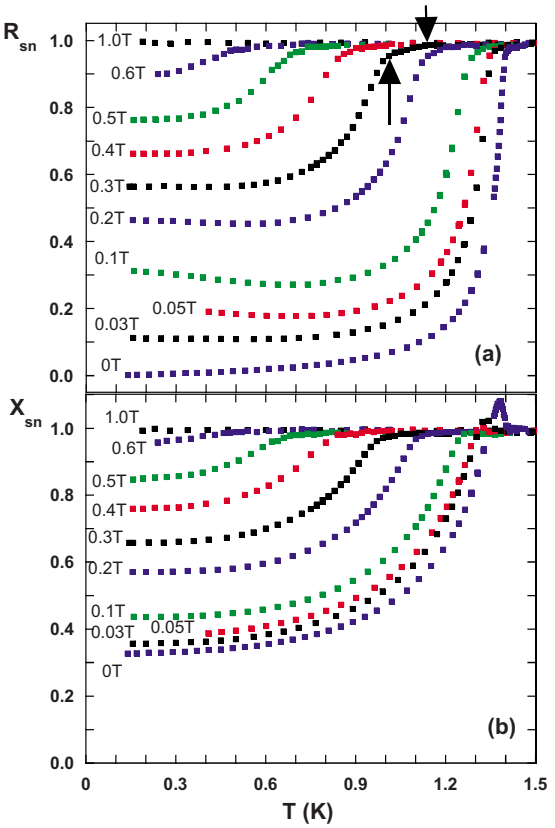

FIG. 6. (Color online) Measurements of (a) R_{sn} and (b) X_{sn} from sample A3 in applied magnetic field, taken at 10.7 GHz. The arrows at 0.3 T indicate the two apparent transitions.

current-induced flux flow.[19] We note that at low temperatures the application of small fields has a significantly larger effect on R_s than on X_s. This implies that losses from the viscous motion of flux lines is important down to the lowest temperatures.

An interesting feature of the mixed-state measurements is the unusual decrease in surface losses on increasing temperature at intermediate fields (30–300 mT). For most type-2 superconductors, increasing temperature would be expected to encourage flux-line depinning and a monotonic increase in losses.

The variation in R_s and X_s with magnetic field at 0.2 and 0.6 K is shown in Fig. 7. At both temperatures R_s and X_s initially increase linearly with field, as predicted by the Coffey-Clem model[9] for microwave-induced flux line motion. The initial linear increase in R_s is larger than that of X_s. This implies that flux flow is more important than flux pinning at this frequency.[19] On increasing the field, R_s rapidly approaches X_s, with an approximately $B^{1/2}$ dependence, consistent with a flux-flow resistivity $\sim(B/B_{c2})\rho_n$ in the mixed state. A more detailed study of the temperature, field, and frequency dependence of the microwave properties in the mixed state will be presented in a subsequent publication.

The measurements of R_{sn} and X_{sn} in Fig. 6 suggest two phase transitions at two distinct temperatures. The first transition, which occurs at a quite distinct temperature when plotted on an expanded scale, we identify with the onset of surface superconductivity[20] at T_{c3}, which occurs above the

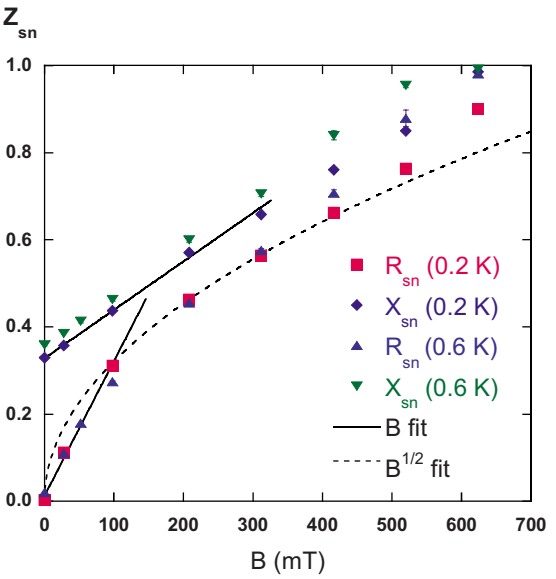

FIG. 7. (Color online) Measurements of R_{sn} and X_{sn} as a function of applied magnetic field taken at 0.2 and 0.6 K from sample A3 at 10.7 GHz.

bulk transition to the mixed state at $T_{c2}(B)$. These are indicated by arrows at the two transition temperatures for the $R_{sn}(B=0.3\ \mathrm{T})$ data.

Figure 8 shows the two phase transitions more clearly for the A3 field data. Below the lower transition, R_{sn} was fitted to a second-order temperature dependence. Above the bulk phase transition, R_{sn} was fitted to a linear dependence and R_{sn} was constant in the normal state. The two phase transitions were determined by the intersections of these lines. The phase diagram derived from the two transitions is shown in Fig. 9 with the solid lines showing fits to a $1-t^2$ dependence. These give values for $B_{c2}(0)=694\pm19$ mT and $B_{c3}(0)=863\pm29$ mT, where the former is in good agreement with the measurements of Matsushita *et al.*[3]

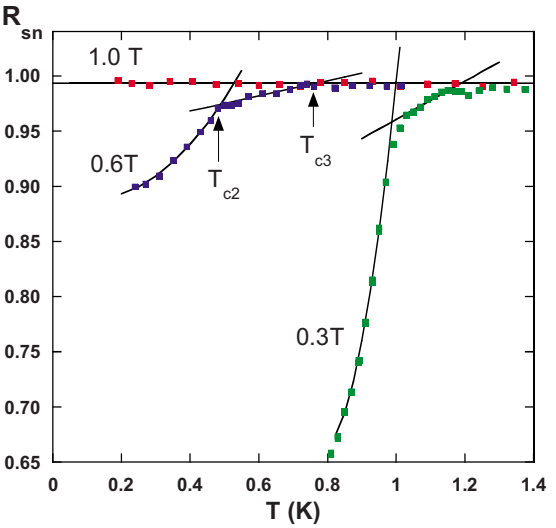

FIG. 8. (Color online) R_{sn} for sample A3 in representative magnetic fields at 10.7 GHz. The intersection of the fitting lines (see text) gives the temperatures of the upper (T_{c3}) and lower (T_{c2}) phase transitions.

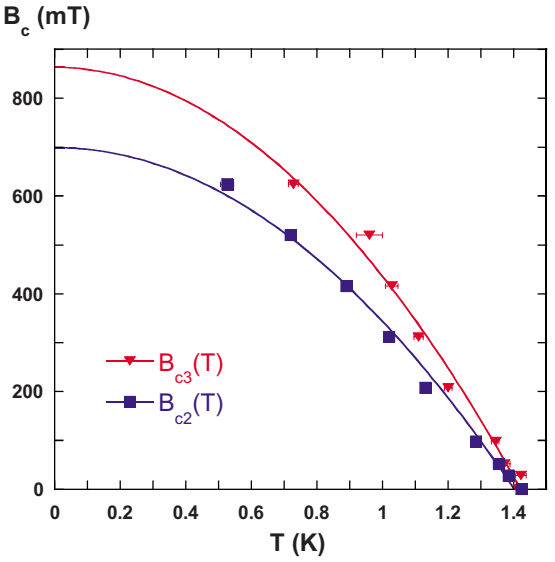

FIG. 9. (Color online) The phase diagram of sample A3 from 10.7 GHz mixed-state measurements, where the apparent upper and lower temperature transitions are plotted. Also included are the fits using $B_c(T)=B_c(0)(1-t^2)$.

A similar B_{c3} effect was observed in measurements on a clean Nb sample, shown in Fig. 10, with a ratio of $B_{c3}/B_{c2}=1.72\pm0.14$ in close agreement with the predicted value[20] of 1.69. The ratio observed in our measurements on Tl(1.4%)PbTe of $B_{c3}(0)/B_{c2}(0)=1.24\pm0.05$ is somewhat lower. This is not unexpected as the value of $B_{c3}(0)$ is strongly dependent on the angle between the applied field and the surface,[21] varying from 1.69 when the field is parallel to the surface to unity when the field is perpendicular. We have already noted that the sample surface is far from smooth, which would lead to a lower value of $B_{c3}(0)$.

V. SUMMARY

Microwave measurements suggest that Tl(1.4%)PbTe is a conventional type-II BCS *s*-wave superconductor. For our best sample at low temperatures, there was no evidence for any significant T or T^2 power-law dependence characteristic of *p*- and *d*-wave superconductors. Furthermore, evidence for surface superconductivity above $T_{c2}(B)$ strongly implies conventional *s*-wave superconductivity, as no such effects have ever been observed for *p*- or *d*-wave superconductors.

Using the independent measurements of the bulk conductivity in the normal state, we deduce a value for $\lambda(0)=1.9\pm0.2$ μm for our best sample, in excellent agreement with predictions based on the measured Hall coefficient assuming a rigid-band model. From the temperature dependence of the microwave properties we derive a superconducting fraction $[\lambda(0)/\lambda(T)]^2$ that falls somewhat below the weak-coupling limit for a BCS superconductor in the dirty limit. This is not unlike the behavior observed in MgB_2, which can be attributed to a two-band superconductor. However, unlike MgB_2, there are no symmetry conditions preventing interband hybridization in Tl-doped PbTe, so such an explanation seems unlikely.

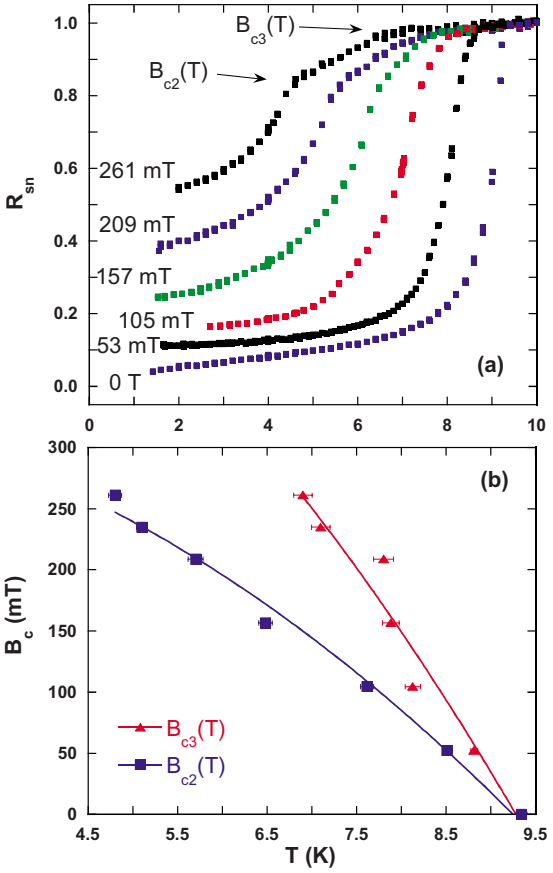

FIG. 10. (Color online) (a) Magnetic field measurements at 8.5 GHz of R_{sn} for a clean sample of Nb. (b) The corresponding phase diagram, where the upper T_c values correspond to B_{c3} and the lower to B_{c2}. Also included are the fits using $B_c(T)=B_c(0)(1-t^2)$.

The derived values of $\sigma_1(T)/\sigma_1(T_c)$ exhibit pronounced frequency-dependent peaks rather larger than the coherence peaks predicted by BCS. However, we note that the derived values for both $[\lambda(0)/\lambda(T)]^2$ and $\sigma_1(T)/\sigma_1(T_c)$ could be made to fit to the BCS predictions if we assumed a value for $\lambda(0)$ of 2.7 μm. This increased value can be obtained from the data, if we assume an increased surface resistance over that of the bulk by $\sim$50%. Although this seems high, it could be caused by weak-link surface properties remaining in even our highest-quality sample or by surface roughness, as observed in other materials.[22,23] This emphasizes the likely sensitivity of all microwave measurements to material-dependent surface properties.

Recent angular resolved photoelectron spectroscopy (ARPES) measurements[24] suggest limitations of the rigid-band model and may account for an increased $\lambda(0)$ value from that predicted from Hall measurements. In the same study, there was no evidence for an impurity band, which has been previously suggested to account for the high T_c in this material.[1] Measurements of the microwave properties in the mixed state exhibit a strong temperature and field dependence of both R_s and X_s consistent with microwave-induced flux flow across the whole frequency range.

ACKNOWLEDGMENTS

We are grateful to F. Marsiglio for helpful discussions and

software for interpreting $\sigma_1(T)/\sigma_1(T_c)$ plots. We would also like to thank E. M. Forgan for his critical reading of this manuscript. This research has been funded by the EPSRC of the United Kingdom. Work at Stanford University is supported by the Department of Energy, Office of Basic Energy Sciences under Contract No. DE-AC02-76SF00515.

[1] S. A. Nemov and Y. I. Ravich, Phys. Usp. **41**, 735 (1998).
[2] Y. Matsushita, H. Bluhm, T. H. Geballe, and I. R. Fisher, Phys. Rev. Lett. **94**, 157002 (2005).
[3] Y. Matsushita, P. A. Wianecki, A. T. Sommer, T. H. Geballe, and I. R. Fisher, Phys. Rev. B **74**, 134512 (2006).
[4] C. M. Varma, Phys. Rev. Lett. **61**, 2713 (1988).
[5] M. Dzero and J. Schmalian, Phys. Rev. Lett. **94**, 157003 (2005).
[6] P. J. Baker, R. J. Ormeno, C. E. Gough, Z. Q. Mao, S. Nishizaki, and Y. Maeno, Phys. Rev. B **80**, 115126 (2009).
[7] W. N. Hardy, D. A. Bonn, D. C. Morgan, R. Liang, and K. Zhang, Phys. Rev. Lett. **70**, 3999 (1993).
[8] D. N. Basov, R. Liang, D. A. Bonn, W. N. Hardy, B. Dabrowski, M. Quijada, D. B. Tanner, J. P. Rice, D. M. Ginsberg, and T. Timusk, Phys. Rev. Lett. **74**, 598 (1995).
[9] B. B. Jin, N. Klein, W. N. Kang, H.-J. Kim, E.-M. Choi, S.-I. Lee, T. Dahm, and K. Maki, Phys. Rev. B **66**, 104521 (2002).
[10] W. A. Huttema, B. Morgan, P. J. Turner, W. N. Hardy, X. Zhou, D. A. Bonn, R. Liang, and D. M. Broun, Rev. Sci. Instrum. **77**, 023901 (2006).
[11] S. Sridhar and W. L. Kennedy, Rev. Sci. Instrum. **59**, 531 (1988).
[12] R. J. Ormeno, M. A. Hein, T. L. Barraclough, A. Sibley, C. E. Gough, Z. Q. Mao, S. Nishizaki, and Y. Maeno, Phys. Rev. B **74**, 092504 (2006).
[13] C. E. Gough and N. J. Exon, Phys. Rev. B **50**, 488 (1994).
[14] M. Tinkham, *Introduction to Superconductivity*, 2nd ed. (McGraw-Hill, New York, 1996).
[15] W. Zimmermann, E. Brandt, M. Bauer, E. Seider, and L. Genzel, Physica C **183**, 99 (1991).
[16] F. Marsiglio, Phys. Rev. B **44**, 5373 (1991).
[17] B. B. Jin, T. Dahm, A. I. Gubin, E.-M. Choi, H. J. Kim, Sung-IK Lee, W. N. Kang, and N. Klein, Phys. Rev. Lett. **91**, 127006 (2003).
[18] A. A. Golubov, A. Brinkman, O. V. Dolgov, J. Kortus, and O. Jepsen, Phys. Rev. B **66**, 054524 (2002).
[19] M. W. Coffey and J. R. Clem, Phys. Rev. B **45**, 9872 (1992).
[20] D. Saint-James and P. G. de Gennes, Phys. Lett. **7**, 306 (1963).
[21] P. G. de Gennes, *Superconductivity of Metals and Alloys* (W. A. Benjamin, New York, 1966).
[22] S. P. Morgan, J. Appl. Phys. **20**, 352 (1949).
[23] Z. Wu and L. E. Davis, J. Appl. Phys. **76**, 3669 (1994).
[24] K. Nakayama, T. Sato, T. Takahashi, and H. Murakami, Phys. Rev. Lett. **100**, 227004 (2008).